A&A 545, C2 (2012)
DOI: 10.1051/0004-6361/201117624e

Astronomy & Astrophysics

Corrigendum

Variations on a theme – the evolution of hydrocarbon solids

II. Optical property modelling – the optEC$_{(s)}$ model⋆

A. P. Jones[1,2]

[1] Institut d'Astrophysique Spatiale, CNRS, IAS UMR 8617, 91405 Orsay, France
e-mail: Anthony.Jones@ias.u-psud.fr
[2] Université Paris Sud, IAS UMR 8617, 91405 Orsay, France

A&A 540, A2 (2012), DOI: 10.1051/0004-6361/201117624

Key words. dust, extinction – ISM: general – errata, addenda

In the computation of the complex refractive index data for the original published version of this article, and in the following article Jones (2012), there was an error in the calculation of the IR band intensities. This error results in small changes in the 3 μm region bands and an underestimation of the band strengths and continua at longer wavelengths for hydrogen-rich a-C:H materials ($X_{\rm H} \gtrsim 0.23 \equiv E_{\rm g} \gtrsim 1$ eV). The conclusions of the paper are unchanged, except as indicated in the following, where an updated version of the relevant figure and, if necessary, the accompanying text is given. The section headings and figure numbers are the same as those used in the originally-published paper. The refractive index data that were originally made available through the CDS have now been replaced with corrected data.

Additionally, there was an error in the overly-complicated reasoning in the deduction of the a-C(:H) particle photo-processing time-scales in Sect. 5.1 of this paper and also in Sect. 5.2 of the following paper (Jones 2012). The photo-processing time-scale is simply the inverse of the photo-darkening rate, $\Lambda_{\rm UV,pd}$, given in Eq. (31). A new and modified version of Sect. 5.1, which replaces the previously published version, is given below.

4.3. The addition of IR bands into the k determination

In Fig. 8 the band gap colour-coding for the data were reversed. The correct caption is now given but the data in this figure are unaffected by the error noted above.

Figure 9 shows the updated refractive index data for bulk a-C:H materials. The most significant differences are apparent in k and occur for large band gap materials with $E_{\rm g} \gtrsim 1$ eV. The IR band strengths for $\lambda > 4\,\mu$m and the long-wavelength continua are enhanced with respect to the previous results. The real part of the refractive index, n, is not significantly affected.

⋆ Data files are only available at the CDS via anonymous ftp to cdsarc.u-strasbg.fr (130.79.128.5) or via http://cdsarc.u-strasbg.fr/viz-bin/qcat?J/A+A/545/C2

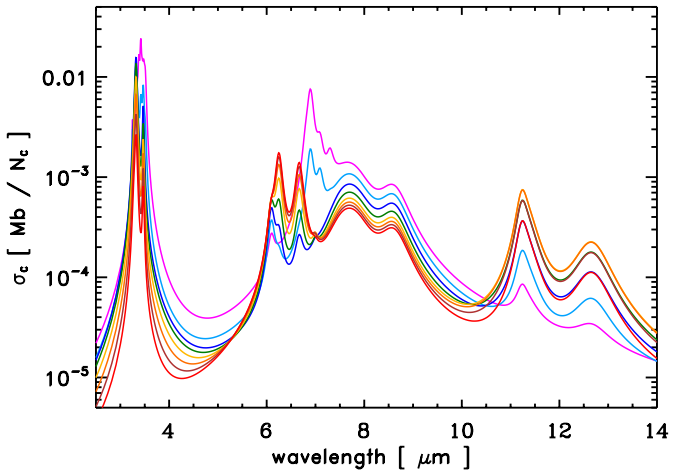

Fig. 8. The adopted wavelength-dependent IR cross-section per carbon atom, $\sigma_{\rm C}$, in Mb (1 Mb = 10^{-18} cm^2) for the eRCN model. The upper curves (violet) are for the H-rich, wide band gap materials and the cross-sections, in the 8 μm region, decrease with decreasing $X_{\rm H} \equiv E_{\rm g}$ from top to bottom – $E_{\rm g}$ = 2.5 (violet), 2.25 (cobalt), 2.0 (blue), 1.75 (green), 1.5 (yellow), 1.25 (orange), 1.0 (brown) and 0.75 eV (red).

4.5. A detailed look at the optEC$_{(s)}$ data

The optEC$_{(s)}$ a-C:H data in Fig. 11 have been updated.

5.1. a-C(:H) processing time-scales

A key question here is: what are the critical photo-processing time-scales that determine the evolution of a-C(:H) materials in the ISM? We now examine this is some detail but return to the issue again in a following paper where we consider the added complication of size effects.

In Fig. 15 we show the depth, d_1 (in nm), at which the optical depth, τ, for photons of a given energy is unity (i.e., $\tau = 1$), for the derived a-C(:H) optical properties. What this shows is that, for all the derived materials, photons with $E \gtrsim 7$ eV are able to

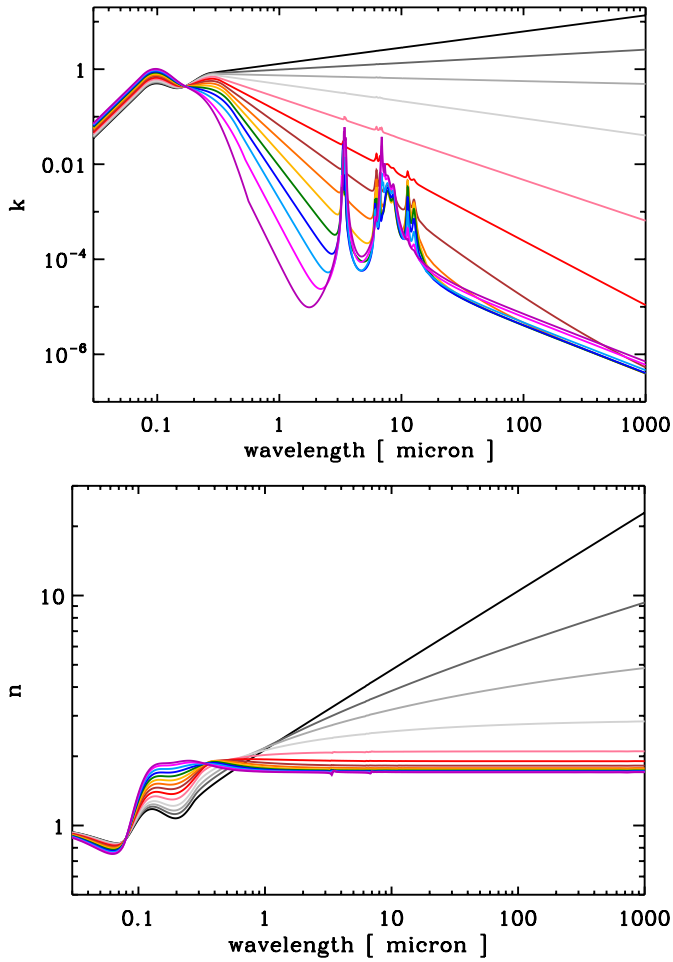

Fig. 9. The imaginary part, k (*upper*), and derived real part, n (*lower*), of the refractive index data for the suite of a-C(:H) materials predicted by the optEC$_{(s)}$ model as a function of E_g (see Table 1 for the line colour-coding).

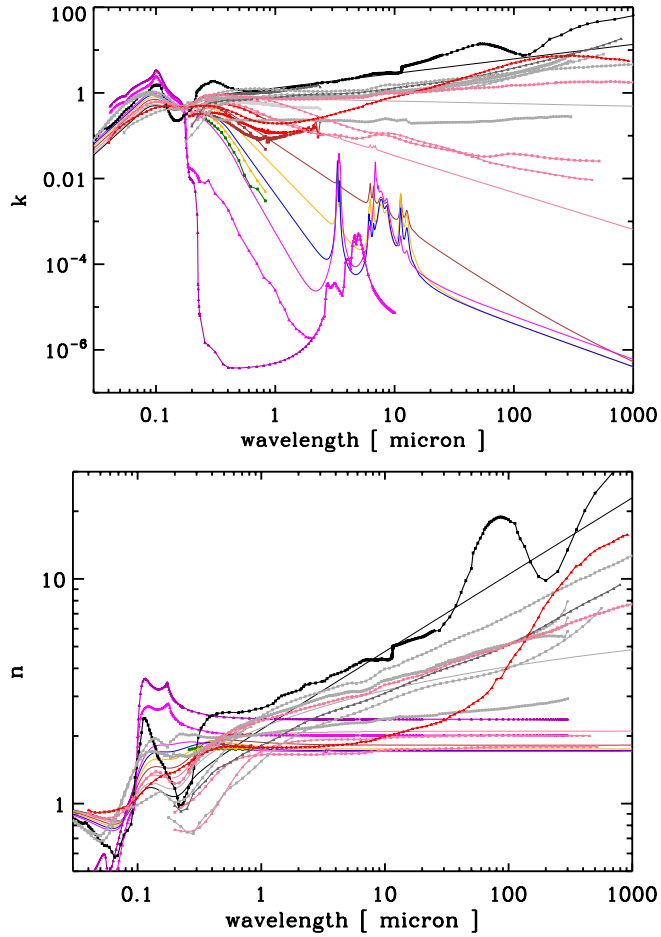

Fig. 11. The smooth, coloured lines show the optEC$_{(s)}$ model-derived imaginary (*top*) and real (*bottom*) parts of the refractive index (large band gap, violet, to low band gap, grey). The lines with data points are the laboratory-measured and model-derived data (see references earlier for the sources). The upper black lines with data points show the data for graphite (Draine & Lee 1984) and the purple and violet lines with data points show the data for diamond (Edwards & Philipp 1985; Lewis et al. 1989).

penetrate the entire particle volume for grains smaller than a few tens of nm in radius. This then also implies that the surfaces of larger grains can only be UV/EUV photo-processed to depths of the order of a few tens of nm by photons with energies greater than ∼7 eV. Such photons, above some threshold energy, will then lead to a-C(:H) grain photo-darkening (photo-processing).

We can estimate a UV/EUV photo-darkening rate, $\Lambda_{\rm UV,pd}$, for carbonaceous dust subject to a given radiation field using

$$\Lambda_{\rm UV,pd} = F_{\rm EUV}\ \sigma_{\rm CH-diss.}\ Q_{\rm abs}(a,E)\ \epsilon, \qquad (31)$$

where $F_{\rm EUV}$ is the dissociating photon flux, $\sigma_{\rm CH-diss.}$ is the CH bond photo-dissociation cross-section, $Q_{\rm abs}(a,E)$ is the particle absorption efficiency and ϵ is a photo-darkening efficiency, which takes into account that photon absorption can also lead to heating and fluorescence (e.g., Sorrell 1990). Based on CH_4 photo-dissociation cross-section studies in the EUV (Welch & Judge 1972; Gruzdkov et al. 1994) we adopt a value of $\sigma_{\rm CH-diss.} = 10^{-19}$ cm^2 centred at ∼107 nm (11.6 eV) and (somewhat conservatively) assume a bandwidth of 33 nm (10−13.6 eV). At UV/EUV wavelengths the photon flux, $F_{\rm EUV}$, appropriate to the local ISRF, can be approximated by $F_{\rm EUV} \approx 10^6$ photons cm^{-2} s^{-1} nm^{-1} (Henry 2002). Integrated over the assumed 33 nm bandwidth for the photo-dissociation cross-section, this then yields $F_{\rm EUV} \simeq 3 \times 10^7$ photons cm^{-2} s^{-1}.

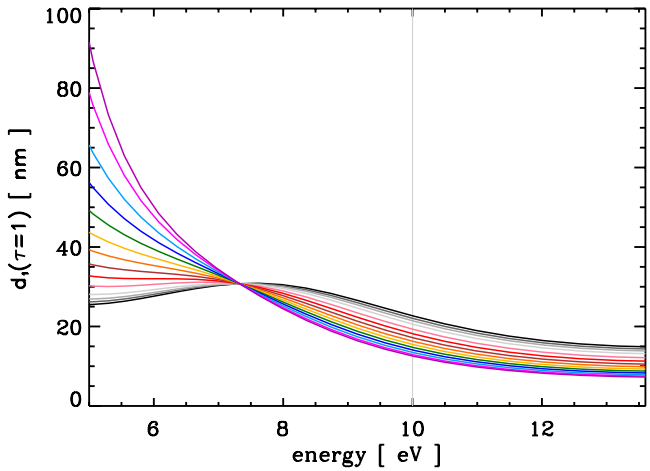

Fig. 15. The depth, d_1, at which $\tau = 1$ for optEC$_{(s)}$ model data. The vertical grey line marks the assumed lower limit for photons capable of photo-dissociating CH bonds in the assumed a-C(:H) materials.

For large grains at these wavelengths $Q_{\rm abs}(a,\ {\rm EUV}) \sim 1$ (i.e., the short-wavelength, linear behaviour in the $\lambda Q_{\rm abs}(a,\ {\rm EUV})/a$ plot in Fig. 16 below). The photo-darkening (or aromatisation)

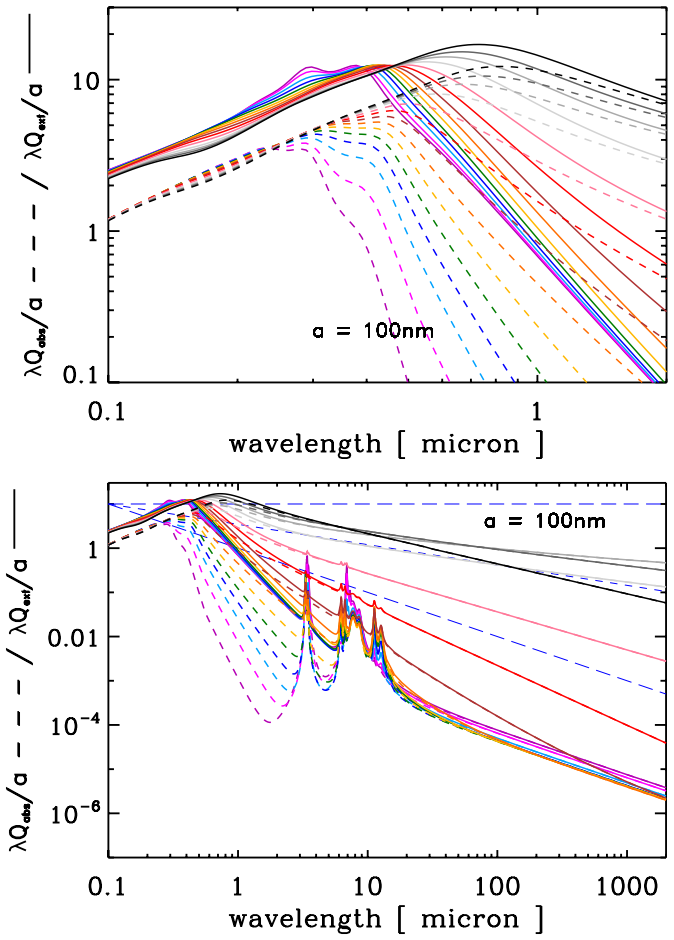

Fig. 16. The optEC$_{(s)}$ model extinction and absorption coefficient data, for clarity plotted as $\lambda Q_{\rm ext}/a$ (solid lines) and $\lambda Q_{\rm abs}/a$ (dashed lines), as a function of $E_{\rm g}$ and wavelength for 100 nm radius particles. From top to bottom on the right the dashed blue lines indicate wavelength dependencies, $\lambda^{-\beta}$, where $\beta = 1$, 1.5 and 2.

time-scale for the outer ≃20 nm of large a-C(:H) particles, $\tau_{\rm UV,pd}$, is then simply the inverse of the photo-darkening time-scale, i.e.,

$$\tau_{\rm UV,pd} \approx (F_{\rm EUV}\, \sigma_{\rm CH-diss.}\, Q_{\rm abs}(a,\lambda)\, \epsilon)^{-1} \approx \frac{10^4}{Q_{\rm abs}(a,\lambda)\, \epsilon} \quad {\rm yr}. \quad (32)$$

If we assume a *per bond* photo-darkening efficiency of $\epsilon = 0.1$, rather than the *per grain* photofission efficiency of 10^{-3} adopted by Sorrell (1990), this yields an ≈20 nm outer-layer photo-darkening time-scale of $\approx 10^5$ yr for large a-C(:H) grains ($a > 20$ nm) in the diffuse ISM. In photo-dissociation regions where the local radiation field can be orders of magnitude over that of the diffuse ISM (e.g., a factor of $\simeq 10^4$ higher for the Orion PDR) these timescales will be significantly shorter. For example, in a PDR with a radiation field 100 (10^4) times that of the diffuse ISM, the outer-layer photo-darkening timescales reduce to $\approx 10^3$ yr (≈10 yr) for large particles. However, in all of these cases the complete photo-processing of the particle is not possible because core material, at depths greater than a few tens of nm, is likely to be unaffected by photo-darkening. Thus, the large carbonaceous grains in the ISM can retain an H-rich interior, as indicated by observations (e.g., Dartois et al. 2004a,b).

The above a-C:H UV processing can also perhaps be considered to engender a sort of band gap "velocity", i.e., $dE_{\rm g}/dt$, which will principally depend upon the local ISRF in the diffuse ISM or given PDR and that only apply to the outer few tens of nm of large particles ($a > 20$ nm). The band gap "velocity", $dE_{\rm g}/dt$, derived from the above, can be expressed as

$$\frac{dE_{\rm g}}{dt} \approx \Lambda_{\rm UV,pd}\, E_{\rm g}(t) \approx 10^{-4}\, Q_{\rm abs}(a,\lambda)\, \epsilon\, E_{\rm g}(t) \quad \left[{\rm eV\ yr^{-1}}\right], \quad (33)$$

which yields a band gap velocity of $\approx 10^{-4}\ \epsilon\ E_{\rm g}(t)$ eV yr^{-1}, where $E_{\rm g}(t)$ is the band gap at time t.

However, we note that the above determination may only give an upper limit to the a-C(:H) aromatisation time-scale because it concerns only the direct photo-dissociation of CH bonds by EUV photons. To this must be added the thermal effects due to photon absorption leading to grain heating to temperatures sufficiently high for H atom loss by thermal annealing to occur.

Thermal processing effects on amorphous hydrocarbons, and the associated kinetics, have been studied in detail by Duley (1996). Using the data of Smith (1984) he showed that, for H atom loss leading to band gap closing, the reaction can be described in terms of a thermally activated process, i.e.,

$$E_{\rm g}(t) = E_{\rm g}^0 {\rm e}^{-k_1 t}, \quad (34)$$

where $E_{\rm g}^0$ eV is the initial band gap (taken to be 2.2 eV) and the rate constant $k_1 = A{\rm e}^{-\Delta H/T}$ (where $A = 6.8\,{\rm s}^{-1}$ and the activation energy $\Delta H = 8000 \pm 2000$ K). With this approach Duley (1996) finds that, for a temperature of 350 K (typical of the extended atmospheres of evolved stars such as IRC+10216), band gap closure (≡aromatisation) can occur on a time-scale of ≈10 yr. Thus, it appears that a thermal processing effect could be important but only if sufficiently high temperatures can be maintained long enough for thermally-driven aromatisation to occur. For grains in the ISM or in PDRs, where grain temperatures are considerably lower than 350 K for large particles in thermal equilibrium with the ISRF ($T \simeq 20$ K), or can only be achieved for very short time-scales in stochastically-heated small particles (for periods of the order of a few seconds every month, i.e., ≈one millionth of their time), the aromatisation time-scales will be considerably longer than 10 yr and probably of the order of, at least, several millions of years. Given that thermal processing is probably only going to be important for stochastically-heated, small a-C(:H) grains we will re-examine this process when we specifically consider grain size effects.

5.3. a-C(:H) extinction and absorption

The data in Figs. 16–18 have been re-calculated based on the corrected complex indices of refraction for a-C(:H). The plot axis intervals are the same as in the originally-published versions in order to allow a direct comparison. The effects of the increased band strengths and enhanced continua at long wavelengths ($\lambda \gtrsim 20\,\mu$m), in large band gap ($E_{\rm g} \gtrsim 1$ eV) a-C:H materials, are evident in Fig. 16.

In Fig. 17 the corrected data do not lead to any significant changes other than the enhanced bands at the shortest wavelengths.

For a-C:H materials with band gaps larger than ∼1 eV Fig. 18 now shows a weaker effect and slightly lower absolute values of β at FIR-mm wavelengths. The changes are most marked for $E_{\rm g} = 1$–1.5 eV materials and for β in the $\lambda \sim 100\,\mu$m region. Hence, the last sentence of the last itemized point should read:

– ... As the band gap further reduces ($E_{\rm g} \sim 1.5\,{\rm eV} \rightarrow -0.1$ eV) β first increases to ≈2.7 for $E_{\rm g} = 1$ eV, drops to ≈1.3 at $E_{\rm g} = 0.1$ eV, and then rises to 1.7 for the smallest band gap material with $E_{\rm g} = -0.1$ eV.

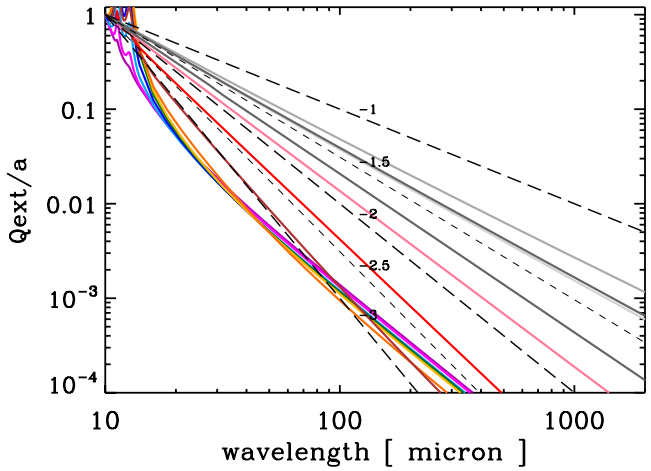

Fig. 17. The optEC$_{(s)}$ model extinction/absorption coefficient data at FIR-mm wavelengths, plotted as Q_{ext}/a and normalised at 10 μm, as a function of E_g for 100 nm radius particles. From top to bottom, the grey dashed lines indicate wavelength dependencies, $\lambda^{-\beta}$, where β = 1, 1.5, 2, 2.5 and 3.

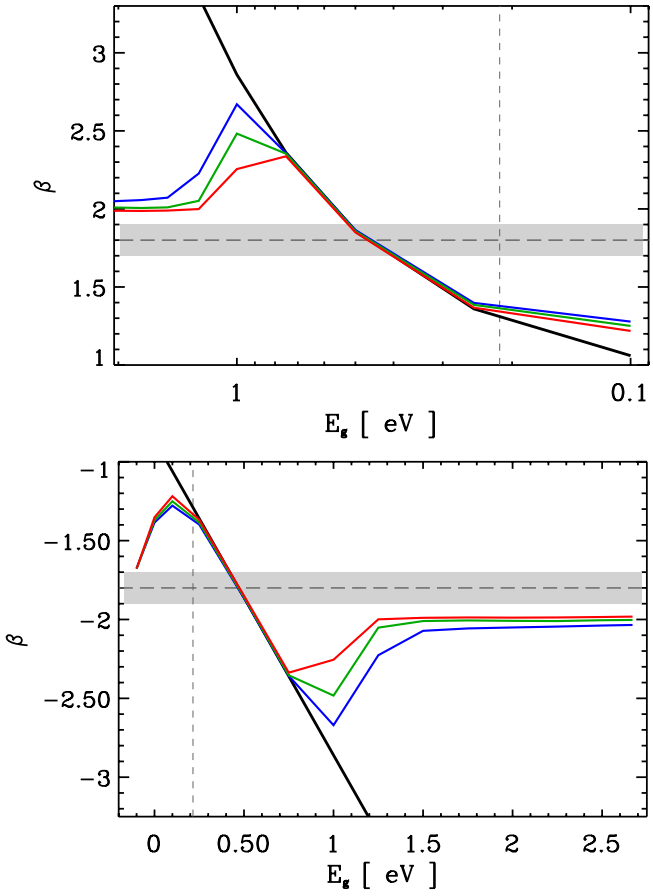

Fig. 18. The predicted emissivity slope, β, at FIR-mm wavelengths as a function of E_g for 100 nm radius particles: blue (at 100 μm), green (at 300 μm) and red (at 1 mm); lower, middle and upper lines, respectively.

In the upper plot in Fig. 18 the same $\beta(E_g)$ data is shown plotted in logarithmic form over a narrower range of E_g in order to allow a comparison with β vs. T_{dust} plots, where T_{dust} could be considered a proxy for E_g, implying that higher band gap materials are to be found in lower dust temperature-higher extinction regions, as might be expected by the accretion of increasingly

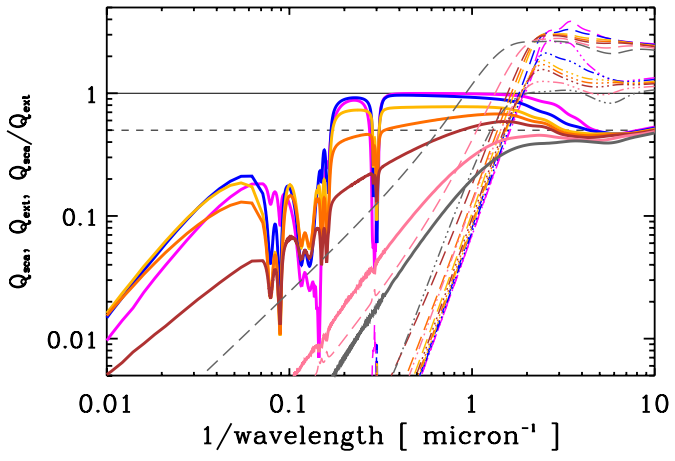

Fig. 19. Q_{ext} (dashed), Q_{sca} (triple-dotted-dashed) and Q_{sca}/Q_{ext} (solid lines) as a function of E_g (0, 0.5, 1.0, 1.25, 1.5, 2.0 and 2.5 eV, from bottom to top) for grains of radius a = 100 nm.

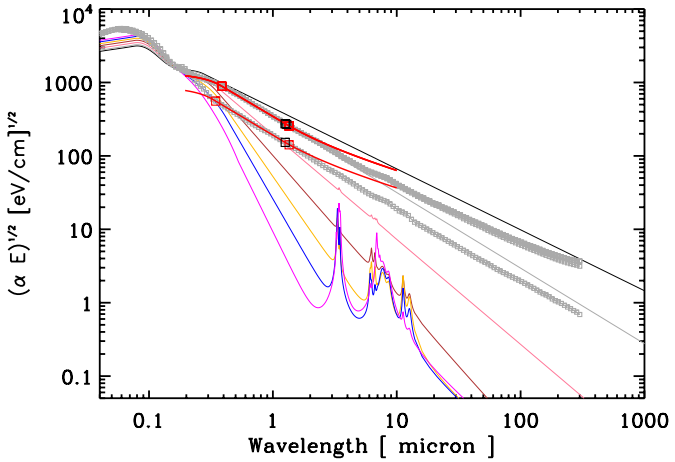

Fig. A.2. As per Figs. 5 and A.1 but for the Rouleau & Martin (1991) data.

hydrogen-rich a-C:H materials in denser regions of the ISM (e.g., Jones et al. 1990).

5.4. Scattering by a-C(:H) grains at mid-IR wavelengths

The first part of the second paragraph of this section should now read:

In Fig. 19 we show Q_{ext} and Q_{sca}, and also the ratio of scattering to extinction Q_{sca}/Q_{ext}, as a function of E_g for 100 nm grains. What this figure shows is, that for a fixed grain size, large band gap a-C(:H) materials ($E_g \geqslant 2$ eV) exhibit almost pure scattering behaviour at wavelengths from 0.5 to 5 μm (0.2–2 μm^{-1}), with sharp downturns at the positions of the strong IR C–H resonances in the 3 μm region. We note that the scattering fraction (see Fig. 19) decreases as the band gap of the material decreases but is still significant for materials with band gaps as low as 1.5 eV...

Appendix A: Tauc analysis of the available data

The a-C:H data in the Tauc analysis wavelength (right hand) plots presented in Figs. A.2 to A.4 have been corrected.

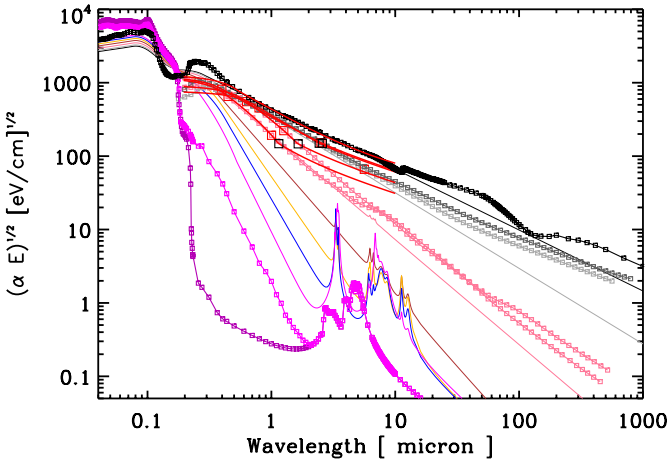

Fig. A.3. As per Fig. A.1 but for the Jena DDOP amorphous carbon data. Also shown for comparison are the data for graphite using the usual $\frac{1}{3}\epsilon_{\perp} + \frac{2}{3}\epsilon_{\parallel}$ approximation (black lines, Draine & Lee 1984) and diamond (purple and violet lines, Edwards & Philipp 1985; Lewis et al. 1989, respectively).

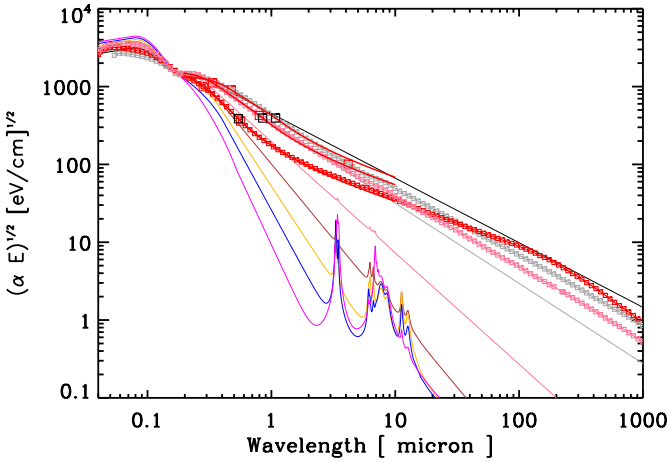

Fig. A.4. As per Fig. A.1 but for the Zubko et al. (1996) data.

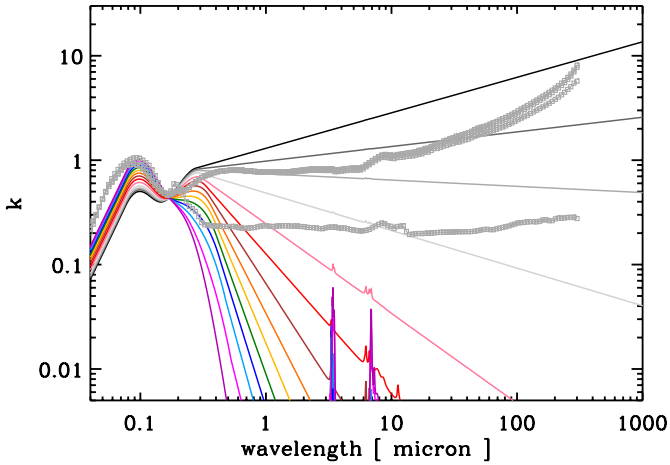

Fig. B.3. Same as Fig. B.1 but for the Rouleau & Martin (1991) data.

Appendix B: The derived optical constants compared with the available data

The imaginary part of the complex indices of refraction, k, in Figs. B.3 to B.5 have been corrected. The corresponding changes in real parts of the complex refractive indices, n, are not discernable in this type of plot and these figures are therefore not reproduced here.

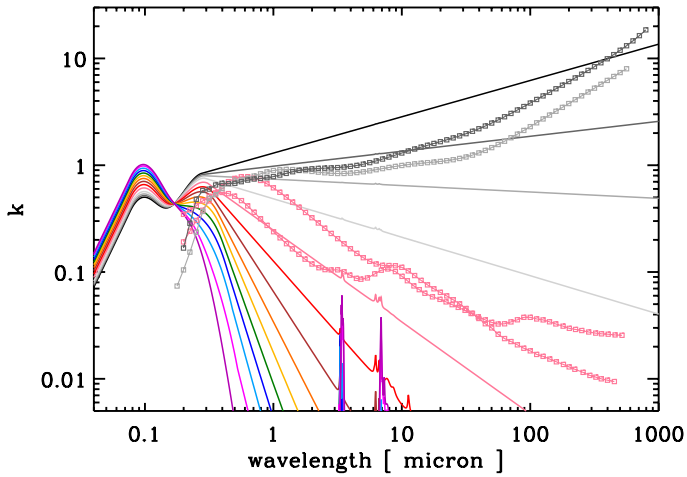

Fig. B.4. Same as Fig. B.1 but for the Jena DDOP amorphous carbon data.

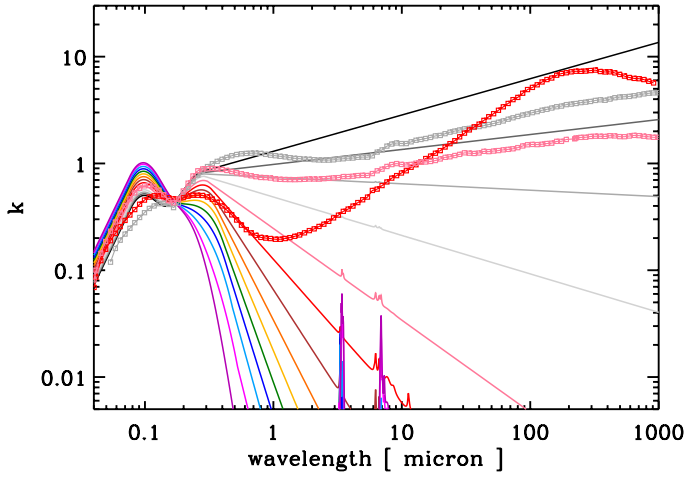

Fig. B.5. Same as Fig. B.1 but for the Zubko et al. (1996) data.

References

Dartois, E., Marco, O., Muñoz-Caro, G. M., et al. 2004a, A&A, 423, 549
Dartois, E., Muñoz Caro, G. M., Deboffle, D., & d'Hendecourt, L. 2004b, A&A, 423, L33
Draine, B. T., & Lee, H. M. 1984, ApJ, 285, 89
Duley, W. W. 1996, MNRAS, 283, 343
Edwards, D. F., & Philipp, H. R. 1985, Handbook of Optical Constants of Solids, ed. E. D. Polik (New York: Academic Press), 665
Gruzdkov, Y. A., Watanabe, K., Sawabe, K., & Matsumoto, Y. 1994, Chem. Phys. Lett., 227, 243
Henry, R. C. 2002, ApJ, 570, 697
Jones, A. P. 2012, A&A, 542, A98
Jones, A. P., Duley, W. W., & Williams, D. A. 1990, QJRAS, 31, 567
Lewis, R. S., Anders, E., & Draine, B. T. 1989, Nature, 339, 117
Rouleau, F., & Martin, P. G. 1991, ApJ, 377, 526
Smith, F. W. 1984, J. Appl. Phys., 55, 764
Sorrell, W. H. 1990, MNRAS, 243, 570
Welch, A. R., & Judge, D. L. 1972, J. Chem. Phys., 57, 286
Zubko, V. G., Mennella, V., Colangeli, L., & Bussoletti, E. 1996, MNRAS, 282, 1321